PNAS
www.pnas.org

Supporting Information for

Dynamic redox balance directs the oocyte-to-embryo transition via developmentally controlled reactive cysteine changes

Boryana Petrova, Keke Liu, Caiping Tian , Maiko Kitaoka, Elizaveta Freinkman, Jing Yang, and Terry L. Orr-Weaver

This PDF file includes:

Supporting text
Supporting references
Figs. S1 to S6

Other supplementary materials for this manuscript include the following:

Datasets S1 to S6

www.pnas.org/cgi/doi/10.1073/pnas.1807918115

Supporting Information Text

SUPPORTING RESULTS

Metabolic perturbations in dhd mutant embryos. We analyzed whether aspects of metabolism, unrelated to redox, are altered in oocytes or embryos in the absence of DHD. PCA analysis of metabolomics analysis did not distinguish differences between stage 14-enriched ovaries or 0-1h embryos from transheterozygous dhd^{P8}/dhd^{J5} mutant females versus those from corresponding sibling controls (Fig. S4B). In oocytes, with our cutoff of $p<0.01$ and FDR<0.1, pathway analysis did not reveal significantly affected processes in *dhd* mutants (Supporting Data File 6). In embryos, however, several pathways were significantly impacted (Fig. S4C and Supporting Data File 6). Notably, several amino acid biosynthesis pathways or the pantothenate and CoA metabolic pathway were significantly different. Due to difficulty in obtaining sufficient material, we were not able to perform this analysis using unfertilized activated eggs, and thus differences between embryos from *dhd* mutant and control mothers could be due to the cell cycle block in *dhd* mutants. In conclusion, DHD likely plays a very restricted, redox-specific role in the metabolic regulation of the oocyte-to-embryo transition.

DHD is highly enriched in oocytes. Quantitative mass spectrometry analysis of protein changes at oocyte maturation and egg activation indicated massive remodeling of the oocyte proteome, exposing potential factors involved in these developmental transitions (1, 2). A compelling observation was that DHD is a maternally deposited protein with the top five highest degree of change at the oocyte-to-embryo transition. It has a 30-fold increase during oocyte maturation and a 40-fold decrease at egg activation (1, 2). As these changes paralleled DHD's redox role, we first sought to narrow the developmental window of DHD expression. We generated DHD transgenic fly lines carrying transgenes with the *dhd* promoter and upstream regulatory regions and either an N-terminal or a C-terminal eGFP or a C-terminal 3xFLAG tag ($FLAG_3$) fused to full length DHD. The most highly expressing C-terminal $FLAG_3$ or N-terminal eGFP-tagged lines

were able to rescue the *dhd*^{J5} null allele and were used for further analysis. eGFP-DHD showed a dramatic increase in protein levels at oocyte maturation with levels being highest in mature MI-arrested stage 14 oocytes (Fig. S6A). A sharp decrease was observed in early 0-1h embryos. Thus, this transgene recapitulates the previously reported changes (1, 2).

Next, we defined the precise timing of eGFP-DHD degradation. We monitored protein changes of eGFP-DHD transgene using the *in vitro* activation egg system (Fig. S6A). CycB levels started to decrease at 20min after activation, indicating initiation of first meiotic anaphase. In contrast, eGFP-DHD protein levels decreased at 60min, a time point at which the majority of embryos have completed the meiotic divisions. Thus, DHD is destabilized after completion of meiosis. This conclusion is supported further by the observation that DHD is stabilized in *cort* mutant embryos, which arrest before completion of meiosis, at the metaphase II to anaphase II transition (1). These results indicate that DHD is highly enriched in oocytes and thus could be required before and/or during completion of meiosis.

DHD has additional roles besides sperm chromatin decondensation. Initially we confirmed the role of DHD in sperm chromatin decondensation by using transgenic male flies carrying GFP Protamine A or B fusions. We stained embryos for the presence of sperm tail and scored fertilized eggs (Fig. S6B, C). We observed that the paternal pronucleus was still condensed and associated with GFP-Protamines in 18% or 27% of 0-1h embryos from *dhd*^{P8}/*dhd*^{J5} or *dhd*^{J5}/*dhd*^{P8} transheterozygous mutant females, respectively. This fraction diminished in 0-2h embryos. Subsequent stages of fertilization, marked by the paternal chromatin having a decondensed morphology and associated tubulin aster, increased in later embryo collections, from 20% or 14% in 0-1h collections to 50% or 56% in 0-2h. In addition to these defects, the fraction of unfertilized embryos, based on sperm tail absence, in either *dhd* transheterozygous allele combination was higher than in control (15% vs 1% in control). We conclude that early steps of fertilization are considerably delayed in *dhd* mutant embryos as reported previously (3, 4). Additionally, *dhd* mutants arrest with decondensed paternal chromatin unable to form the first zygotic spindle.

In 0-2h embryo collections, we noticed that although the majority of *dhd* mutant eggs had formed polar bodies, those were often aberrant: 30% and up to 50% from $dhd^{J5}/Df(1)dhd81$ and $dhd^{P8}/Df(1)dhd81$, respectively (Fig. S6D, E). This was not simply due to disintegration of the polar body, as seen during a prolonged arrest, because defects were observed even in 30min embryo collections (Fig. S6D). We found an increase in ploidy and chromatin hypercondensation or fragmentation among the polar body defects (Fig. S6F). In addition, 13% of $dhd^{J5}/Df(1)dhd81$ embryos were still undergoing meiosis, stages that are rarely observed in control eggs (2%). Finally, we noticed that in the majority of *dhd* mutant eggs, in addition to an aster associated with around 1N DNA content, often up to 2-4 free asters were scattered through the egg cytoplasm (Fig. S6F, G). Taken together, our observations suggest additional defects in *dhd* mutants affecting the integrity of maternal chromatin, microtubule organization and/or meiotic progression.

SUPPORTING MATERIALS AND METHODS

The term "biological replicate" was used to mean a repeat of all of the steps of an experiment, such as independent fly crosses, isolation of oocytes or embryos, preparation and subsequent relevant analysis.

Fly stocks and transgenic lines. To construct a tagged *dhd* gene fusions driven by the genomic promoter, the genomic sequence including *dhd* was amplified by PCR with primers (C-terminus tagged *dhd* left arm - GAGGTCACTAGTCAGTTCGTCCAGCTTGGGTG and CCATGGCGGCCGCTCCACTTCCGCCCGCCTTCACCAGCTTGGCCATC; C-terminus tagged *dhd* right arm – ACGTCGGGCCCGCAGCAATCCTGCCCAGCAATTAG and GAGGTCACGCGTCTCTCGTTGAACATGCGACG ; N-terminus tagged *dhd* left arm - GAGGTCACTAGTCAGTTCGTCCAGCTTGGGTG and ACCATGGCGGCCGCTTTTATGTCGCGAGGATTAGCAAAG; N-terminus tagged *dhd* right arm - TGTACAAGGGGCCCGGCGGAAGTGGAATGGCATCCGTACGCACCATGAAC and

GAGGTCACGCGTCTCTCGTTGAACATGCGACG) and cloned into pMT-eGFP-puro (Addgene). The $FLAG_3$-tagged construct was generated by swapping the NotI-ApaI flanked GFP with a synthetic oligo (GCGGCCGCCGACTACAAAGACCATGACGGTGATTATAAAGATCATGACATCGATTACAAGGAT GACGATGACAAGTAAGGGCCC). The resulting constructs were then swapped into pCasPeR4 (5), digested with *SpeI* and *HpaI*. pCasPeR4 *dhd-egfp, egfp-dhd or* $FLAG_3$*-dhd* were injected into w^{1118} embryos and transgenics were recovered by P element transposition (Genetic Services, Sudbury, MA). The table below summarizes transgene functionality, expression levels, and tagged protein localization.

transgene	**expression**	**rescue**	**localization**
DHD-$FLAG_3$_1	not tested	no larva or adults	not tested
DHD-$FLAG_3$_2	not tested	not tested	not tested
DHD-eGFP_3	not tested	not tested	nurse cell cytoplasm and nuclei, possibly nucleolar; oocyte cytoplasm and nucleus
DHD-eGFP_4	very high	not tested	oocyte cytoplasm and nucleus
DHD-eGFP_5	high	no larva or adults	not tested
DHD-eGFP_6	not tested	not tested	not tested
eGFP-DHD_7	good	some larva and adults	oocyte cytoplasm and nucleus
eGFP-DHD_8	weak	some larva and adults	nurse cell cytoplasm and nuclei; oocyte cytoplasm

			and nucleus
eGFP-DHD_9	good	some larva and adults	oocyte cytoplasm and nucleus
DHD-$FLAG_3$_10	good	not tested	not tested
DHD-$FLAG_3$_11	very weak	not tested	not tested
DHD-$FLAG_3$_12	weak	some larva and adults	not tested

Oocyte and embryo collections. Ovaries and egg chambers were hand dissected from fattened females in Isolation buffer (55mM NaOAc, 40mM KOAc, 110mM sucrose, 1.2mM $MgCl_2$, 1mM $CaCl_2$, 100mM Hepes; final pH 7.4 with NaOH). Fertilized embryos were collected for 1h, dechorionated in 50% bleach and washed in water, and briefly in embryo wash buffer (0.9% NaCl, 0.03% Triton X-100). Unfertilized activated eggs were collected for 1 or 2h from virgin females mated to sterile *twine*^{HB5} males that do not make sperm (6, 7), dechorionated and washed as above.

For immunoblotting, five oocytes, unfertilized activated eggs or embryos in 5 μL embryo wash buffer were frozen in liquid N_2 and stored at -80˚C. After addition of 5 μL 4X Laemmli sample buffer (LSB), they were homogenized on ice, sonicated briefly in a Bioruptor (Diagenode) at 4ºC with 30sec on and 30sec off settings and boiled for 5 min.

For immunofluorescence, embryos were fixed and stained with DAPI as in (8). Mature oocytes were fixed and stained as in (9), except DAPI was used. Alpha-Tubulin was stained either with 1:1000 of DM1 anti-alpha-Tubulin antibodies (T9026, Sigma Aldrich, St. Louis, MO) and 1:1000 of anti-mouse Alexa-fluor 488-labeled secondary antibodies (Invitrogen, A11029) or 1:1000 of anti-alpha-Tubulin antibodies (Accurate Chemical & Scientific Corp, YSRTMCA77P) and 1:1000 anti-rat Alexa-fluor 488-labeled secondary antibodies (Invitrogen, A11006). Gamma-Tubulin was stained with 1:1000 of anti-gamma-Tubulin antibodies (Sigma-Aldrich, T5326) and 1:1000 of anti-mouse Alexa-fluor 647-labeled secondary antibodies

(Invitrogen, A21242). The sperm tail was stained with a monoclonal antibody from Tim Karr. Sample scoring was on a Nikon ECLIPSE Ti microscope with Plan Fluor 10x or Plan Apo 20x objectives.

In vitro egg activation. Stage 14 oocytes were activated as previously described (9-12). Stage 14 oocytes were isolated in Isolation buffer (55mM NaOAc, 40mM KOAc, 110mM sucrose, 1.2mM $MgCl_2$, 1mM $CaCl_2$, 100mM Hepes; final pH 7.4 with NaOH) from virgin females enriched for mature oocytes (10) and activated in freshly prepared Activation buffer (3.3mM NaH_2PO_4, 16.6mM KH_2PO_4, 10mM NaCl, 50mM KCl, 5% PEG 8000, 2mM $CaCl_2$, brought to pH 5.4 - 6.4 with 1:5 NaOH:KOH). If DTT treatment was used, 5mM DTT was added to the Activation buffer. When activated oocytes were collected at more than 25 min after initiation of activation, the oocytes were washed with H_2O, transferred and incubated further in modified Zalokar's buffer (9mM $MgCl_2$, 10mM $MgSO_4$, 2.9mM NaH_2PO_4, 0.22mM NaOAc, 5mM glucose, 34mM glutamic acid, 33mM glycine, 2mM malic acid, 7mM $CaCl_2$, pH 6.8 (with 1:1 NaOH:KOH)). Activated oocytes were dechorionated and selected for successful activation by treatment with 50% bleach for 90sec then washed with H_2O and embryo wash buffer. Fixation and DAPI staining were as described above for embryos. The meiotic stages were defined by chromosome structure (9). For immunoblotting, activated eggs were washed in embryo wash buffer, and 10-30 eggs were frozen in 5-15µL embryo wash buffer in liquid N_2 and stored at -80˚C. After addition of 5-15µL of 4xLSB buffer, they were homogenized on ice, sonicated for 10 cycles (30sec on, 30sec off) and their protein concentration was determined by Bradford assay (BioRad, Hercules, CA). The equivalent of 5µg protein (5 ooyctes) was loaded in 2x LSB for Western blotting after 5min boiling.

Immunoblotting. Samples were separated by 8% or 10% SDS-PAGE and transferred to Immobilon polyvinylidene fluoride membranes (EMD Millipore, Billerica, MA) or nitrocellulose (Whatman, Protran, WHA10401316). Proteins were detected by ECL2 (Thermo Fisher Scientific, Waltham, MA) and visualized with ChemiDoc XRS+ (BioRad, Hercules, CA) or X-ray film (Labscientific, XAR ALF 2025). If

membranes were to be reprobed with another antibody, they were stripped with stripping buffer (0.2M Glycine, pH 2.5 and 1% SDS).

Primary and secondary antibodies used were:

antibody	**dilution**	**source**
mouse monoclonal anti-CycB	1:200	Developmental Studies Hybridoma Bank, Iowa City, IA
guinea pig anti-GFP	1:10.000	a gift from Mary-Lou Pardue, MIT
rat anti-α tubulin (YOL1/34)	1:10.000	AbD Serotec, Raleigh, NC
mouse anti-FLAG M2	1:1000	Sigma-Aldrich, St. Louis, MO
HRP-conjugated anti-rabbit IgG	1:10.000	Jackson ImmunoResearch, West Grove, PA
HRP-anti-guinea pig IgG	1:10.000	Jackson ImmunoResearch, West Grove, PA
HRP-anti-mouse IgG	1:10.000	Jackson ImmunoResearch, West Grove, PA
HRP-anti-rat IgG	1:10.000	Jackson ImmunoResearch, West Grove, PA

To increase the sensitivity and specificity of the antibodies for CycB and FLAG, we used Signal Enhancer Hikari (Nacalai USA, San Diego, CA).

Pulldowns and quantitative MS-analysis for identification of enriched proteins. The *dhd* or *trx*-2 ORFs were cloned into pET28-b (Merck KGaA, Germany). Cysteine 34 in DHD or cysteine 35 in Trx-2 were mutated to serine using site directed mutagenesis (QuickChange Lightning, Aligent Technologies, USA). HIS-DHD-C34S or HIS-Trx-2-C35S proteins were expressed in BL21 and purified by Ni-sepharose according to manufacturer procedures (Qiagen, Germany). A total of 1.5mg extracts were prepared as described for immunoprecipitation experiments. A total of 200µg recombinant HIS-DHD-C34S or HIS-Trx-2-C35S proteins were re-bound to 150µL Ni-magnetic beads (Dynabeads, Life Technologies, Carlsbad, CA) and incubated with extract for 1h at 4^{o}C. Control pulldowns were beads alone. Bound proteins were eluted with 10mM DTT for 30min at 25^{o}C. Samples were treated for MS analysis as in Hara *et al* (13). Peptide

labeling with TMT 8plex (Thermo Fisher Scientific, Waltham, MA) was performed per manufacturer's instructions. Only peptides with a Mascot score greater than or equal to 25 and an isolation interference less than or equal to 30 were included in the quantitative data analysis. TMT quantification was obtained using Proteome Discoverer and isotopically corrected per manufacturer's instructions.

Immunoprecipitation for DHD interaction mapping. 0-1h embryos or ovaries enriched for stage 14 oocytes from flies expressing an *eGFP-dhd* construct or *OrR* controls were frozen in liquid nitrogen, briefly homogenized in NP40 buffer (25mM Tris, pH 7.4, 0.5mM EDTA, 0.5% NP40, 1X Complete EDTA-free protease inhibitor cocktail (Roche, Indianapolis, IN), 2X PhosSTOP (Roche, Indianapolis, IN), 250nM okadaic acid and sonicated in a Bioruptor (Diagenode) at 4^{o}C for 15 cycles at 30sec on and 30sec off. After spinning at 13.3 krpm at 4^{o}C for 5 min, the supernatants were transferred to new tubes and the protein concentration adjusted to 3 mg/mL. eGFP-DHD was immunoprecipitated from 3 mg of the protein extracts with 25µL GFP-TRAP_MA beads (Chromotek, Planegg-Martinsried, Germany) for 30min. After three washes with NP40 buffer and one wash with NP40 buffer supplemented with 300mM NaCl, proteins were eluted by incubation in 0.2M Glycine, pH2.5, for 10 sec. The elutate was neutralized with 1M Tris-HCl (pH 8) and proteins were precipitated by 10% TCA for 30min on ice. The pellet was washed with ice-cold acetone and frozen in liquid nitrogen.

Sample Preparation for Mass Spectrometry. Precipitated elutions were washed overnight in 50% methanol/water. These were washed once more with 47.5/47.5/5 % methanol/water/acetic acid for 2h, dehydrated with acetonitrile and dried in a speed-vac. Reduction and alkylation of disulfide bonds then were carried out by the addition of 30µL 10mM dithiothreitol (DTT) in 100mM ammonium bicarbonate for 30min. The resulting free cysteine residues were subjected to an alkylation reaction by removal of the DTT solution and the addition of 100mM iodoacetamide in 100mM ammonium bicarbonate for 30 min to form carbamidomethyl cysteine. These were then sequentially washed with aliquots of acetonitrile, 100mM ammonium bicarbonate and acetonitrile and dried in a speed-vac. Proteins were enzymatically digested by

the addition of 300ng of trypsin or chymotrypsin in 50mM ammonium bicarbonate overnight at 37^{o}C with gentle shaking. The resulting peptides were extracted by the addition of around 50µL of 50 mM ammonium bicarbonate with gentle shaking for 10 min. The supernatant from this was collected in a 0.5ml conical autosampler vial. Two subsequent additions of 47.5/47.5/5% acetonitrile (ACN)/water/formic acid with gentle shaking for 10min were performed with the supernatant added to the 0.5mL autosampler vial. The organic solvent was removed and the volumes were reduced to 15µL using a speed-vac for subsequent analyses.

Chromatographic separation of peptides for interaction partner analysis. The digestion extracts were analyzed by reversed phase high performance liquid chromatography (HPLC) using Waters NanoAcquity pumps and autosampler (Waters, Milford, MA) and a ThermoFisher Orbitrap Elite mass spectrometer (ThermoFisher Scientific, Waltham, MA) using a nano flow configuration. A 20mm x 180 micron column packed with 5 micron Symmetry C18 material (Waters, Milford, MA) using a flow rate of 15 µL per minute for three min was used to trap and wash peptides. These were then eluted onto the analytical column that was self-packed with 3.6 micron Aeris C18 material (Phenomenex, Torence, CA) in a fritted 20 cm x 75 micron fused silica tubing pulled to a 5 micron tip. The gradient was isocratic 1% A Buffer for 1 minute 250 nL min^{-1} with increasing B buffer concentrations to 15% B at 20.5 min., 27% B at 31min and 40% B at 36min. The column was washed with high percent B and re-equilibrated between analytical runs for a total cycle time of approximately 53 min. Buffer A consisted of 1% formic acid in water and buffer B consisted of 1% formic acid in acetonitrile.

***Mass spectrometry and data analysis for DHD interaction partners*.** The mass spectrometer was operated in a data dependent acquisition mode, where the 10 most abundant peptides detected in the Orbitrap using full scan mode with a resolution of 240,000 were subjected to daughter ion fragmentation in the linear ion trap using multi stage activation where neutral losses of 97.97, 48.99 or 32.66 m/z below the precursor were

fragmented further (pseudo MS3). A running list of parent ions was tabulated to an exclusion list to increase the number of peptides analyzed throughout the chromatographic run.

Peptides were identified from the MS data using PEAKS Studio 8.0 (Bioinformatics Solutions), Mascot (Matrix Science, Boston, MA) and Sequest (ThermoFisher Scientific, Waltham, MA) algorithms. Species-specific (*Drosophila melanogaster*) Refseq FASTA files were downloaded from NCBI and concatenated to a database of common contaminants (keratin, trypsin, etc). The resulting search results from PEAKS, Mascot and Sequest were then loaded into Scaffold (Proteome Software, Portland, OR).

Statistical analysis for immunoprecipitation analysis (SAINT). Non-specific binders were filtered from the DHD IPs using the SAINT algorithm version 3.4 (14). The protein spectral counts were used as a measure of protein abundance and the data of a bait (DHD) IP versus the control experiments compared. SAINT calculates the probability of true interaction (SAINT score >0.6). Fold-change was further computed as the ratio of median spectral counts observed in DHD pull-downs versus the control experiments. Only those with fold-change >4 were considered as the real bait interactors.

Preparation of IPM probe-labeled proteome samples. Stage 14 enriched ovary or 0-1h embryo collections were obtained as for immunofluorescence, weighed on an analytical balance and kept frozen at -80ºC. Roughly 3-10mg of tissue was lysed in NP40 buffer (without DTT) containing 200 unit/mL catalase (Sigma-Aldrich, St Lous, MO) and 100 μM IPM (Kerafast, EVU111) by sonication for 15 cycles of 30sec on and 30sec off (Bioruptor, Diagenode). The lysate was first incubated at room temperature for 1h with light protection, then 8mM DTT was added and the lysate was incubated for 15min at 75ºC. Finally, 100mM IAA (iodoacetamide, Sigma-Aldrich, I1149) was added and the lysate was incubated at room temperature for 20min with light protection. Proteins were precipitated with methanol/chloroform, resuspended in 50mM ammonium bicarbonate, and the protein concentration was determined as previously described (15). The probe-labeled lysates were digested with trypsin at 37°C overnight. The tryptic digests were desalted with HLB extraction cartridges (Waters) and evaporated to dryness under vacuum. The resulting peptides were

reconstituted in a solution containing 30% ACN at pH ~6. Click chemistry was performed by the addition of 1mM either light or heavy Azido-UV-biotin (1µL of a 40mM stock), 10mM sodium ascorbate (4µL of a 100mM stock), 1mM TBTA (1µL of a 50mM stock), and 10mM $CuSO_4$ (4µL of a 100mM stock). The samples were allowed to react at room temperature for 2h with rotation and light protection. The light and heavy isotopic tagged samples were then mixed immediately following click chemistry. The samples were cleaned by strong cation exchange (SCX) chromatography as previously described (15) and then allowed to interact with pre-washed streptavidin sepharose for 2h at room temperature. The streptavidin sepharose then was washed with 50mM NaOAc (sodium acetate, pH4.5), 50mM NaOAc containing 2M NaCl (pH4.5), and water twice, each time with vortexing and/or rotation to remove non-specific binding substances. The beads were then resuspended in 25mM ammonium bicarbonate. The suspension of streptavidin sepharose was transferred to several glass tubes (VWR) and irradiated with 365 nm UV light (Entela, Upland, CA) for 2h at room temperature with stirring. The supernatant was collected, the volume of photo-released sample was reduced to ~100µL by vacuum centrifugation, and it was desalted with HLB extraction cartridges (Waters). The desalted samples were stored at −20 °C until analysis.

LC-MS/MS Analysis for IPM-labeled peptide analysis. LC-MS/MS analyses were performed on a QExactive plus (Thermo Fisher Scientific) coupled with an EasynLC1000 system (Thermo Fisher Scientific). Samples were reconstituted in 0.1% formic acid and pressure-loaded onto a 2 cm microcapillary precolumn packed with C18 (3 µm, 120 Å, SunChrom, USA). The precolumn was connected to a 12 cm 150 µm-inner diameter microcapillary analytical column packed with C18 (1.9 µm, 120 Å, Dr. Maisch GebH, Germany) and equipped with a homemade electrospray emitter tip. The spray voltage was set to 2.0 kV and the heated capillary temperature to 320°C. The LC gradient consisted of 0min, 7% B; 14min, 10% B; 51min, 20% B; 68min, 30% B; 69−75min, 95% B (A = water, 0.1% formic acid; B = ACN, 0.1% formic acid) at a flow rate of 600 nL/min. MS1 spectra were measured with a resolution of 70,000, an AGC target of 3e6, a max injection time of 20 ms, and a mass range from m/z 300 to 1400. HCD MS/MS spectra were recorded in

the data-dependent mode using a Top-20 method with a resolution of 17,500, an AGC target of 1e6, a max injection time of 60 ms, a 1.6 m/z isolation window and normalized collision energy of 30. Peptides m/z that triggered MS/MS scans were dynamically excluded from further MS/MS scans for 18 s.

Peptide Identification and Quantification for IPM-labeled peptide analysis. Raw data files were searched against the UniProt-Drosophila database. The database search was performed with pFind studio (Version 3.1.11). Precursor ion mass and fragmentation tolerance was 10 and 20 ppm, respectively. The maximum number of modifications allowed per peptide was two, as was the maximum number of missed cleavages allowed. Different modifications of +15.9949 Da (methionine oxidation), +57.0214 Da (iodoacetamide alkylation), and +252.1222 (IPM modification) were searched as variable modifications. A differential modification of 6.0201 Da on IPM-derived modification was used for all analyses. The FDRs were estimated by the program from the number and quality of spectral matches to the decoy database. For all data sets, the FDRs at spectrum, peptide, and protein level were <1%.

Quantification of heavy to light ratios ($R_{H/L}$) was performed using pQuant as previously described, which directly uses the RAW files as the input (15, 16). pQuant calculates $R_{H/L}$ values based on each identified MS scan with a 10 ppm-level *m/z* tolerance window and assigns an interference score (Int. Score, also known as confidence score σ) to each value from 0 to 1. In principle, the lower the calculated Int. Score, the less co-elution interference signal was observed in the extracted ion chromatograms. In this regard, the median of peptide ratios with $\sigma \leq 0.5$ were considered to calculate site-level ratios. Quantification results were obtained from at least three biological replicates with one or two 75 min LC-MS/MS run for each.

LC-MS Metabolomics. Embryos and activated eggs were treated as described above for immunoprecipitation and stored in -80^{o}C. Ovaries were dissected one by one in Isolation buffer, briefly dipped in water to wash away buffer components, and immediately dipped in -80^{o}C methanol kept on dry ice. Only two flies were on a CO_2 pad at a time to minimize exposure (roughly 1min). Multiple samples per

condition and genotype were collected, and roughly equal amounts were pooled based on absolute wet weight measure on an analytical fine balance (Mettler Toledo, Billerica, MA). We noticed that normalization based on exact oocyte or embryo counts, wet weight, total lipid content (determined by LC-MS quantification as described in (17)) or isotopically-labeled valine and phenylalanine led to similar standard deviation and relative differences. Note that ratios between reduced and oxidized metabolites were independent of normalizations. Frozen samples were then extracted in LC/MS-grade MetOH/$ClCH_3$/water at 6:4:3 (Fisher Chemicals, Pittsburgh, PA). For Ellman's reagent derivatization (ELL), 20mM of DNB (D8130, Sigma-Aldrich, St. Louis, MO) was added to LC-MS water. For formic acid (FA) extraction, 0.1M formic acid (94318, Sigma-Aldrich, St. Louis, MO) was added to the water and after homogenization, the solute mixture was neutralized with 15% ammonium bicarbonate (A6141, Sigma-Aldrich, St. Louis, MO). The methanol was supplemented with isotope-labeled standards serving as an internal reference.

Extracted metabolites were separated into polar and lipid fractions and dried in a CentriVap concentrator equipped with a cold trap (Labconco, Kansas City, MO). Polar samples were treated for small molecule LC-MS as previously described (18). MS data acquisition was performed in a range of m/z = 70–1000, with the resolution set at 70,000, the AGC target at $1x10^6$, and the maximum injection time (Max IT) at 20msec. An additional scan (m/z = 220-700) in negative mode only was included to enhance detection of nucleotides. For detection of nicotinamide diadenine nucleotide cofactors, targeted selected ion monitoring (tSIM) scans with an isolation window of width 3.0 m/z were centered at m/z = 665.1243 and m/z = 745.0850 for NAD(H) and NADP(H), respectively. For tSIM scans, the resolution was set at 70,000, the AGC target was $1x10^5$, and the max IT was 250msec. Relative quantitation of polar metabolites was performed with XCalibur QuanBrowser 2.2 (Thermo Fisher Scientific) and TraceFinder software (ThermoFisher Scientific, Waltham, MA) using a 5 ppm mass tolerance and referencing an in-house library of chemical standards. Pooled samples and fractional dilutions were prepared as quality controls and only those metabolites were taken for further analysis, for which the correlation between the dilution factor and the peak area read was

>0.9 were taken for further analysis (high confidence metabolites). Total integrated peak area values were used as readout of relative concentrations after normalizing all values to the averaged factor from all mean centered readouts. Normalizing to the sum of all area reads from either polar or lipid signal lead to similar results. The data were further mean centered for MetaboAnalyst-based statistical analysis (19).

roGFP live-cell imaging. To avoid background from yolk autofluorescence we spun down flies or embryos as described previously (20). For oocytes, 5-7 females were spun at 13k rpm on a bench-top centrifuge in 1mL of Grace's unsupplemented media for 25min. Ovaries were then dissected in Grace's, ovarioles pulled apart and loaded in two wells on LabTek slides (NUNC 155411, Rochester, NY) in 500µL Grace's. For embryos, 0-1h collections were washed and dechorionated as for immunofluorescence. Small holes were then punched on a 6-well culture dish filled with agar-molasses and embryos were oriented to fit longitudinally inside. The dish was spun for 12min at 3600rmp on an Eppendorf 5810R table-top centrifuge (Eppendorf, Germany). Embryos were washed out with Grace's and placed in 1.5mL tubes. To permeabilize the embryos, they were treated for 1min,15sec with a 1:4 dilution of Citrasolv in Grace's (Citrasolv LLC, USA) and washed 7 times with Grace's. Finally, embryos were transferred to two wells on LabTek slides in 500µL Grace's. Treated samples were imaged immediately starting with well 1 (corresponding to before oxidation treatment). Then, 500µL of Grace's supplemented with 2mM DA or 0.6% H_2O_2 was added to it. After imaging the second well (corresponding to before reduction treatment), 500µL of Grace's supplemented with 10mM DTT was added to it. Finally, the DA/ H_2O_2 (well 1 after oxidation) and then DTT treated (well 2 after reduction) were imaged. Imaging took around 30min in total, which corresponded to treatment with oxidizing or reducing reagent for 7min before imaging. Images were taken with fixed exposure times at both 405/535nm and 488/535nm excitation/emission settings on a Nikon ECLIPSE Ti microscope with Plan Fluor 10x or Plan Apo 20x objectives. Three regions of interest were chosen per oocyte or embryo away from any yolk autofluorescence signal and intensities were measured using ImageJ (imagej.nih.gov/ij/). Ratios were averaged in Excel.

DNA-FISH. Ovaries dissected as described above for immunofluorescence were fixed, pre-hybridized, hybridized and washed as previously described (21). Sense probes against *X* or *II* chromosome were designed as in (21) and synthesized with a 5'-Cy3 or Cy5 labels respectively (Sigma-Aldrich, St. Louis, MO). Tissues were mounted and visualized as described above for immunofluorescence.

S2 cells transfection, immunoprecipitation and immunofluorescence. S2 cells were grown in Schneider's (Life Technologies, 21720-024) supplemented with 10% FBS (Sigma Aldrich, F6178-500ML) and penicillin/streptomycin (Life Technologies, 15070063) at 25ºC in suspension. Cells were transfected with Effectene (Qiagen) following manufacturer protocols. For copper-inducible transient or stable transfection, either pMT-puro (Addgene) or pIBU1 (a kind gift from E. Hallacli, Whitehead Institute) was used. Stable cell lines were generated following manufacturer protocols (Qiagen) and positive clones were selected by growing cell in 1mg/mL G418 (pIBU1) for 8 days. eGFP-pIBU1 was first generated by inserting the *egfp* (amplified with: fwd - GGCGGCGGCCGCCATGGTGAGCAAGGGCGAGGAG; rev - ATCCGGCGCGCCTTACTTGTACAGCTCGTCCATG primers) into NotI-AscI cut vector. *dhd* (amplified with: fwd - CAGCTTAATTAAATGGCATCCGTACGCACCATG; rev – CATGGCGGCCGCCGCCTTCACCAGCTTGGCCATC primers) was then inserted into PacI/NotI sites. pMT-$FLAG_3$ was used to insert *no66* (amplified with: fwd – CAAGACTAGTGGCGGAAGTGGAATGAAAAAGGCGACTACTTCC; rev – ATCCGGCGCGCCCTACTTAAACGGCTTCTCGGTC primers) or *cnbp* (amplified with: fwd – CAAGACTAGTGGCGGAAGTGGAATGTCGATGTCTGCCACGTG; rev – GATCCGGCGCGCCCTAGTTCCGTCCGCCCTTCTC primers) into the SpeI/AscI sites. Expression was induced 1d after transfection for 2-3d with 500µM $CuSO_4$. For immunoprecipitation, 1-2x10^6 cells were collected by centrifugation and lysed in NP40 buffer (see above) for 10min on ice. After measuring protein concentration by Bradford assay (BioRad, Hercules, CA), 300 to 500µg extract was incubated with 2.5µL eGFP-TRAP beads (Chromotek) for 30-60min at 4ºC. Bound proteins were washed three times with NP40

buffer, one time with NP40 buffer supplemented with 300mM NaCl, one time with PBS and eluted in 4xLSB by boiling at 95ºC for 5min. For immunofluorescence, S2 cells were seeded on poly-Lysine (Sigma-Aldrich, P4707) coated microscopy slides and fixed for 10min with 4% pFA (16 % el mic grade, Electron Microscopy Scienc Nm 15710). They were then washed several times in PBS, permeabilized by 0.5% Triton X100 and blocked in IF-block buffer (5% BSA, 5% NGS, 0.1%Triton X100 in PBS). Primary antibodies were incubated for 1-3h at RT, the cells washed three times in PBS, and they were then further incubated in Alexa-fluor labeled secondary antibodies or anti-GFP Atto488-labelled nanobodies.

Antibody	Label (nm)	Dilution	Source
anti-FLAG M2	NA	1:1000	Sigma, M8823-1ML
VHH anti eGFP	Atto488	1:1000	Chromotek, gtma-10
anti-mouse	Alexa647	1:1000	Invitrogen, A-31571
anti-rabbit	Alexa568	1:1000	Life Technologies, A-11011

DNA was stained with DAPI for 10min. Cells were mounted and visualized as described above for immunofluorescence.

qPCR analysis. Total RNA and cDNA was prepared from 50 dissected stage 14 oocytes as described (22). Real-time qPCR was performed with primers against target sequences for different TRIP RNAi or GAL4-UAS lines (see table for targets and primers), using Perfecta SYBR Green FastMix (Quanta BioSciences) with an Applied Biosystems 7300 Real-Time PCR machine according to the manufacturer's instructions. PCR values were normalized to levels of *RP49* in control cDNA.

target	**forward primer**	**reverse primer**
dhd	AGCCCCATCACGTCAAGTT	CCATGTCGCATAGAAATCCA

sod1	ATCCGTATGGCAAGGAGCAT	GTCGGTGATGTTGACCTTGG
sod2	CGACACCACCAAGCTGATTC	GGCCTTCTTCAGATCATCGC
cat	CTACACTGAGGATGGCGTCT	GGTGAGGAAGTCCCAGAACA
trxr1	CGAGGAGGCCGAGGATGTTT	GGGCAGGTTCAGATCGTCCA
trx2	TGCGGACCCTGCAAGATGAT	GAAGGTGGGCATGCTGGAGA
zw	TGCAGATCCTCTCGCTGGTG	CAGGGCCTCGATGCTCTTCA
no66	CAGGATCTCGTCGGGCAACT	ATGTGCAGCGAGTGCTGTTG
RP49	CAGTCGGATCGATATGCTAAGC	AATCTCCTTGCGCTTCTTGG

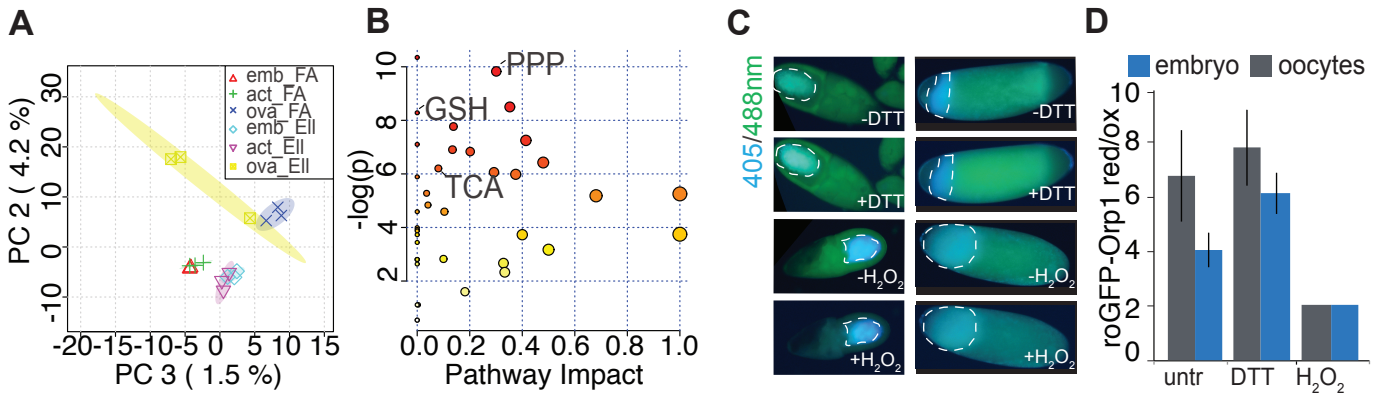

Fig. S1. Redox state changes at the oocyte-to-embryo transition. A.) Principal component analysis by MetaboAnalyst of metabolomics data from extracts from wild-type OrR stage 14-enriched ovaries, unfertilized activated eggs, and 0-1h embryos prepared either by formic acid (FA) or Ellman's (Ell) extraction. B.) Pathway impact analysis from MetaboAnalyst from the Ellman's extraction method comparing control stage 14-enriched ovaries and 0-1h embryo collections. Several pathways that are statistically significantly different ($p<0.01$ and FDR < 0.05) are indicated. PPP – pentose phosphate pathway; TCA – citrate cycle; GSH – glutathione metabolism. C.) Live-cell imaging of roGFP-Orp1 in oocytes or 0-1h embryos from OrR flies before or after treatment with either 10mM DTT or 1% H_2O_2 for 10min. Images were taken at either 405nm (blue false color) or 488nm (green false color) excitation and 535nm emission. Dotted line indicates the position of the partitioned yolk, which was avoided in measurements (see Materials and Methods). All images were adjusted to the same brightness and contrast and taken with the same settings. D.) Samples were treated as depicted in C and the ratio of measurements taken at both channels was normalized to the fully oxidized sample (and arbitrary fixed at 2). Error bars are the standard deviation from three independent biological experiments.

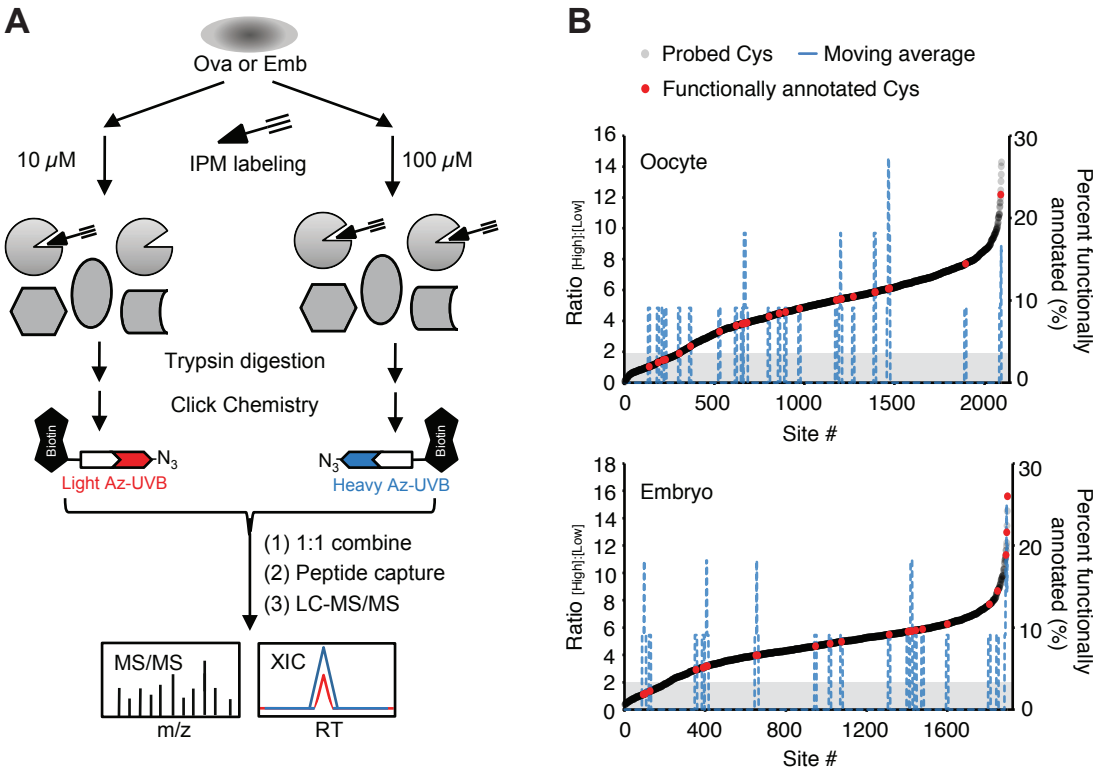

Fig. S2. Cysteine-reactivity profiling of the oocyte-to-embryo transition. A.) Workflow to quantify cysteine-reactivity in the Drosophila ovary and embryo proteome. The Drosophila stage 14-enriched ovary or 0-1h embryo lysates were treated with either 10 μM or 100 μM IPM probe, digested with trypsin, and conjugated to the light or heavy UV-cleavable azido-biotin via click chemistry (CuAAC). The samples were combined and then enriched with streptavidin, and subjected to UV-treatment at 365 nm to release the probe-labeled peptides for LC-MS/MS analysis. B.) Correlation of heavy (100 μM) to light (10 μM) ratios of determined cysteine reactivity from stage14-enriched ovaries (upper panel) or 0-1h embryo collections (lower panel) with functional annotations (red dots) from the UniProt database. Functional annotations include the active site or disulfide bonds. A moving average (window of 11) of functional cysteines is shown as a dashed blue line. Gray shaded area highlights the cysteine reactivity cut off (light/heavy ratio <2).

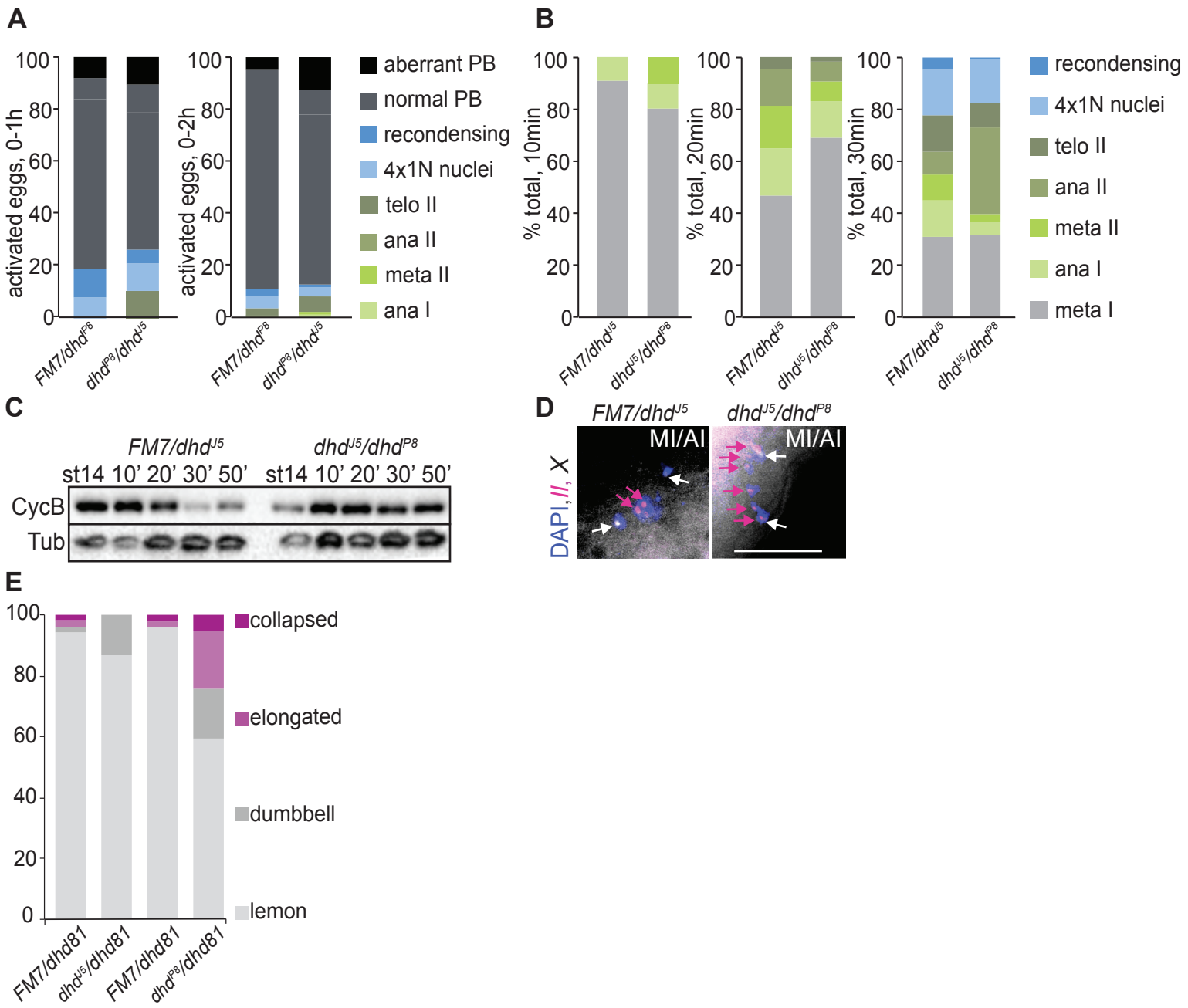
A
activated eggs, 0-1h
activated eggs, 0-2h
100
80
60
40
20
0
FM7/dhdP8
dhdP8/dhdJ5
aberrant PB
normal PB
recondensing
4x1N nuclei
telo II
ana II
meta II
ana I
B
% total, 10min
% total, 20min
% total, 30min
FM7/dhdJ5
dhdJ5/dhdP8
recondensing
4x1N nuclei
telo II
ana II
meta II
ana I
meta I
C
FM7/dhdJ5
dhdJ5/dhdP8
st14 10' 20' 30' 50'
CycB
Tub
D
FM7/dhdJ5
dhdJ5/dhdP8
MI/AI
DAPI, II, X
E
collapsed
elongated
dumbbell
lemon
FM7/dhd81
dhdJ5/dhd81
FM7/dhd81
dhdP8/dhd81

Fig. S3. Characterization of DHD roles in the oocyte-to embryo transition. A.) Quantification of stages in unfertilized activated eggs from 0-1h or 0-2h collections from dhd^{P8}/dhd^{J5} mothers and corresponding sibling controls mated to $twine^{HB5}$ males and stained with DAPI. The four maternal meiotic products (4x1N) were observed to recondense after the completion of the second meiotic division and before the formation of a polar body (PB). B.) Quantification of meiotic progression from 10, 20 or 30min after *in vitro* activation of mature, MI arrested stage 14 oocytes from dhd^{J5}/dhd^{P8} virgins and corresponding sibling controls. This is a representative experiment from three biological replicates. C.) Western blot analysis of Cyclin B (CycB) levels from *in vitro* activated stage 14 oocytes from dhd^{J5}/dhd^{P8} virgins and corresponding sibling controls for the indicated time points. α-tubulin (Tub) was used as a loading control. This is a representative experiment from three biological replicates. D.) Chromosome *X* (white and white arrows) and *II* (magenta and magenta arrows) DNA FISH staining in 30min *in vitro* activated eggs from dhd^{J5}/dhd^{P8} and sibling FM/dhd^{J5} control. The chromosomes from a single activated egg are shown in each panel. Control chromosomes are in a typical configuration for MI/AI, but one or both chromosome *II* in *dhd* mutant embryos are aberrantly stretched or decondensed at MI/AI (six loci are visible – arrows). Scale bar is 20μm. E.) Quantification of MI arrest morphologies in mature, stage 14 oocytes from *dhd* mothers of indicated genotypes ("81" – *Df(1)dhd81;* "*P8*" – dhd^{P8}; "*J5*" – dhd^{J5}) and corresponding sibling controls stained with DAPI. Lemon or dumbbell are normal MI arrest morphologies, whereas elongated and collapsed are rarely observed.

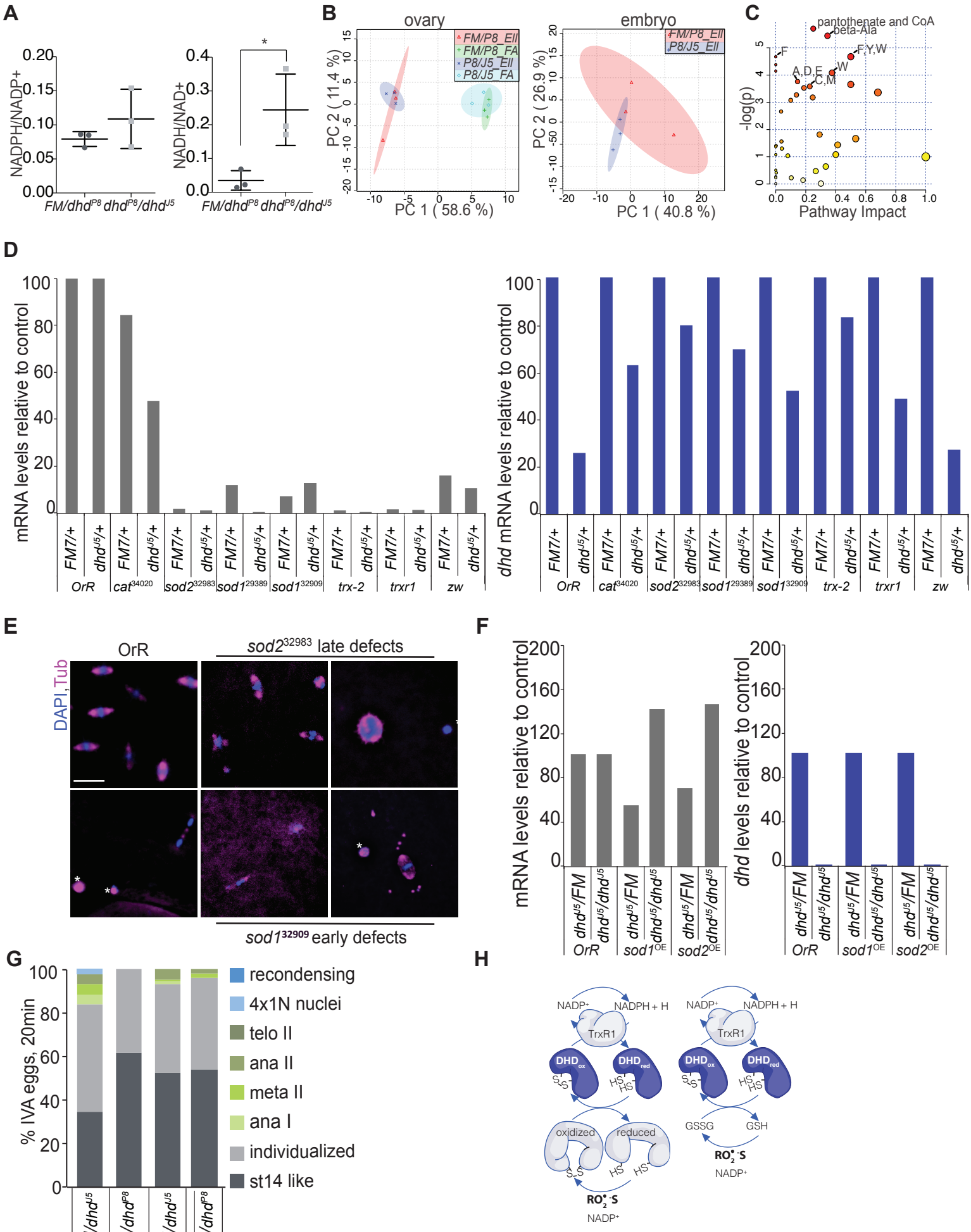
A
NADPH/NADP+
NADH/NAD+
FM/dhdP8 dhdP8/dhdJ5
B
ovary
embryo
FM/P8_EII
FM/P8_FA
P8/J5_EII
P8/J5_FA
PC 1 (58.6 %)
PC 2 (11.4 %)
PC 1 (40.8 %)
PC 2 (26.9 %)
C
pantothenate and CoA
beta-Ala
-log(p)
Pathway Impact
D
mRNA levels relative to control
dhd mRNA levels relative to control
FM7/+
dhdJ5/+
OrR
cat34020
sod232983
sod129389
sod132909
trx-2
trxr1
zw
E
OrR
sod232983 late defects
sod132909 early defects
DAPI, Tub
F
mRNA levels relative to control
dhd levels relative to control
dhdJ5/FM
dhdJ5/dhdJ5
OrR
sod1OE
sod2OE
G
% IVA eggs, 20min
recondensing
4x1N nuclei
telo II
ana II
meta II
ana I
individualized
st14 like
FM/dhdJ5
dhdJ5/dhdP8
-
5mM DTT
H
NADP+
NADPH + H
TrxR1
DHDox
DHDred
oxidized
reduced
GSSG
GSH
NADP+

Fig. S4. Redox control of the oocyte-to-embryo transition. A.): NADPH/NADP+ and NADH/NAD+ ratios measured by LC-MS analysis of formic acid treated extracts from stage 14-enriched ovaries from dhd^{P8}/dhd^{J5} mothers and corresponding sibling controls. "*FM*" denotes the *FM7* balancer. Error bars represent the standard deviation from three independent biological replicates, asterisk – $p<0.1$. B.) Principle component analysis by MetaboAnalyst of dhd^{P8}/dhd^{J5} stage 14-enriched ovaries, or 0-1h embryo extracted by either formic acid (FA) or Ellman's (Ell) methods. "*FM*" denotes the *FM7* balancer. Three biological replicates were analyzed. C.) Pathway impact analysis by MetaboAnalyst of around 70 high-confidence metabolites from Ellman's (Ell) extraction method of dhd^{P8}/dhd^{J5} or corresponding sibling control 0-1h embryo collections. The letters designate metabolic pathways for corresponding amino acids. Three biological replicates were analyzed. D.) qPCR analysis of cDNA from stage 14 oocytes from the indicated lines. The y-axis shows the levels of mRNA from each the *OrR* or RNAi transgenes shown on the x-axis. Values were normalized to the *RP49* mRNA control and are presented relative to mRNA levels from embryos laid by $+/dhd^{J5}$*; Mat(alpha) GAL4* virgin mothers. Right panel - same as on the left except levels of *dhd* mRNA were evaluated. E.) Examples of observed defects in the indicated RNAi lines. 0-1h embryos were stained with DAPI (blue) and anti-α-tubulin (magenta). Asterisk indicates the polar bodies. Scale bar is 20μm. F.) qPCR analysis from indicated lines ("*J5*" – dhd^{J5}). Values were normalized to *RP49* mRNA control and presented relative to mRNA levels from embryos laid by control $+/dhd^{J5}$*; Mat(alpha) GAL4* virgin mothers. The left panel shows the levels of *sod1* or *sod2* mRNA. Right panel - levels of *dhd* mRNA. "*FM*" denotes the *FM7* balancer. G.) Quantification of meiotic progression at 20 min after *in vitro* activation of mature, MI arrested stage 14 oocytes from dhd^{J5}/dhd^{P8} young females and corresponding sibling controls in the presence of 0 or 5mM DTT. "*FM*" denotes the *FM7* balancer. This is a representative experiment from three biological replicates. H.) Schematic representation of proposed redox state control at the oocyte-to-embryo transition in Drosophila. DHD can alter the redox state of specific proteins (left) or globally change redox state through glutathione (right). TrxR1- thioredoxin reductase 1.

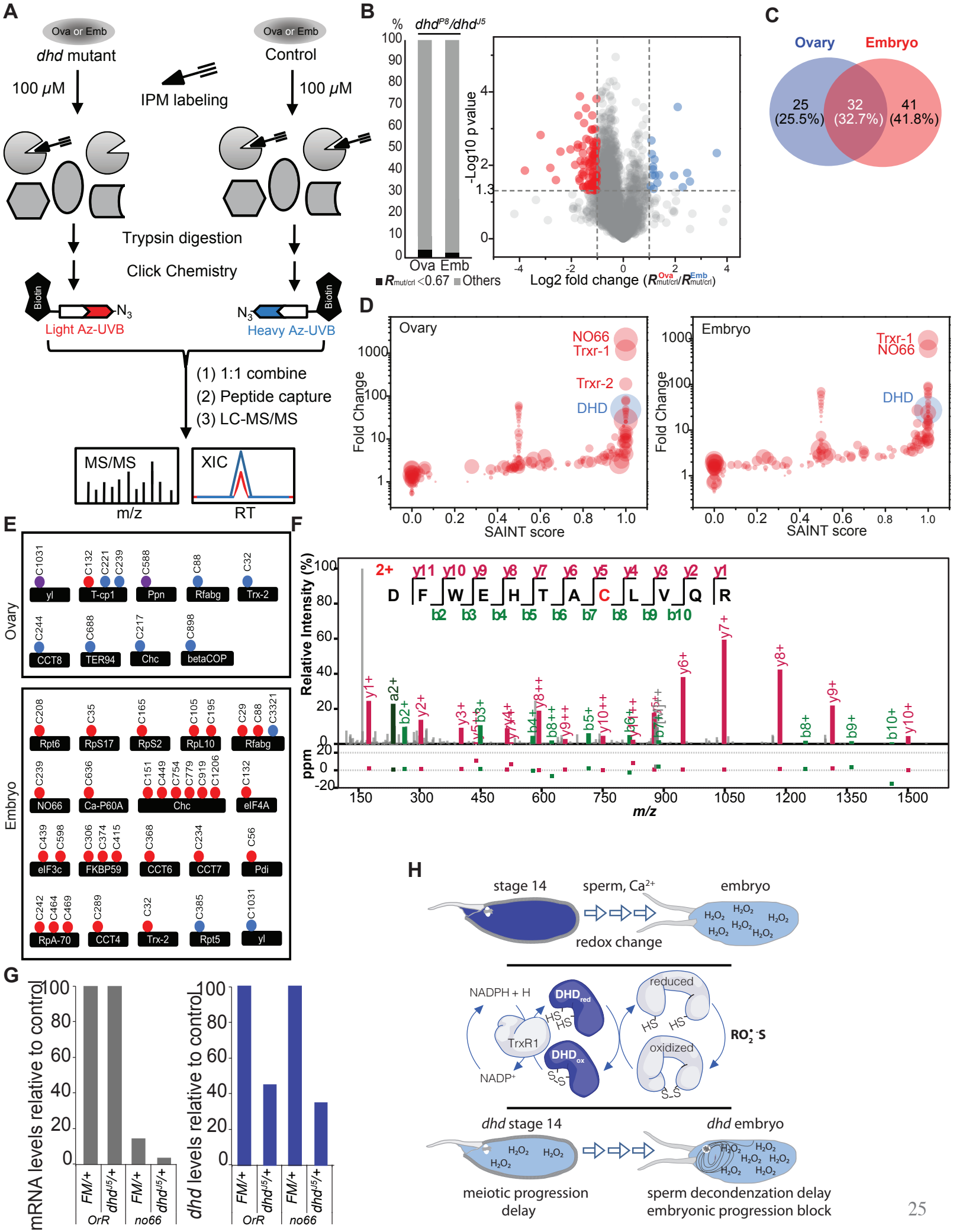
A
Ova or Emb
dhd mutant
Ova or Emb
Control
100 μM
IPM labeling
100 μM
Trypsin digestion
Click Chemistry
Biotin
N3
Light Az-UVB
N3
Biotin
Heavy Az-UVB
(1) 1:1 combine
(2) Peptide capture
(3) LC-MS/MS
MS/MS
m/z
XIC
RT
B
% dhdP8/dhdJ5
Ova
Emb
Rmut/crl <0.67
Others
-Log10 p value
Log2 fold change (ROvamut/crl/REmbmut/crl)
C
Ovary
Embryo
25 (25.5%)
32 (32.7%)
41 (41.8%)
D
Ovary
Embryo
Fold Change
SAINT score
NO66
Trxr-1
Trxr-2
DHD
E
Ovary
yl
T-cp1
Ppn
Rfabg
Trx-2
CCT8
TER94
Chc
betaCOP
Embryo
Rpt6
RpS17
RpS2
RpL10
Rfabg
NO66
Ca-P60A
Chc
eIF4A
eIF3c
FKBP59
CCT6
CCT7
Pdi
RpA-70
CCT4
Trx-2
Rpt5
yl
F
2+
D F W E H T A C L V Q R
Relative Intensity (%)
ppm
m/z
G
mRNA levels relative to control
dhd levels relative to control
FM/+
dhdJ5/+
OrR
no66
H
stage 14
sperm, Ca2+
embryo
redox change
NADPH + H
DHDred
TrxR1
DHDox
NADP+
reduced
oxidized
ROO·S
dhd stage 14
dhd embryo
meiotic progression delay
sperm decondenzation delay
embryonic progression block

Fig. S5. DHD interacts with a diverse set of downstream targets. A.) Workflow to quantify cysteine-reactivity changes between *dhd* mutant and the corresponding sibling control. The lysates obtained from stage 14-enriched ovaries or 0-1h embryos from *dhd* mutant or control mothers were treated with 100 μM IPM probe, digested with trypsin, and conjugated to the light (*dhd* mutant) or heavy (control) UV-cleavable azido-biotin via click chemistry. The samples were combined, enriched with streptavidin, and subjected to 365 nm UV-treatment to release the probe-labeled peptides for LC-MS/MS analysis. B.) Quantitative thiol-reactivity profiling of proteomic cysteines from extracts of stage 14-enriched ovaries and 0-1h embryos recovered from dhd^{P8}/dhd^{J5} or sibling control females. Bar chart (left) showing the distribution of cysteines with a *dhd*-dependent decrease in reactivity ($R_{mut/crl}$ <0.67) in ovaries and embryos. Volcano plot (Right) showing the comparison of the $R_{mut/crl}$ values determined in the two tissues. Log_2 of fold change (ova/emb) is plotted against significance values in $-log_{10}$. All data points are averages from at least three biological replicates. The determined $R_{mut/crl}$ changed more than two-fold in ovaries compared to embryos are highlighted in blue or red respectively. If the fold change of R^{ova}/R^{emb} of a cysteine is higher than two (ie blue) it suggests that the cysteine has a greater DHD-dependent decrease in reactivity in embryos than in ovaries. C.) Venn diagram showing the number and corresponding percentage of specific DHD-interacting proteins recovered from immunoprecipitation experiments and identified to be distinct or shared between ovaries and embryos. The percentage represents the corresponding fraction relative to total. D.) Comparison of the probability of true interaction (x-axis, SAINT score) versus the fold changes of spectral count (y-axis, log scale) for each protein identified in DHD-specific immunoprecipitation experiments as compared to control. The data represent two independent biological replicates (n=2 per condition, eGFP-DHD vs *OrR* control) from stage 14-enriched ovaries or 0-1h embryos. Each point is proportional in size to the number of spectral counts identified. E.) Examples of DHD-specific substrates, found to associate with DHD by immunoprecipitation and to contain cysteines that demonstrated decreased reactivity in *dhd* mutant tissues relative to sibling controls (red: dhd^{J5}/dhd^{P8}; blue: dhd^{P8}/dhd^{J5}; purple: both transheterozygous combination

mutant females). F.) Representative MS/MS spectrum of the IPM-labeled peptide from NO66 C239 (Related to Fig. 5B) G.) Analysis of mRNA levels in stage 14 oocytes of corresponding targets in indicated RNAi lines by qPCR. Left- *RP49* mRNA is shown from *OrR* and *no66* from RNAi and sibling controls. The *no66* mRNA values were normalized to *RP49* mRNA control oligos and presented relative to mRNA levels from control +/+ or *+/dhd^{J5}; Mat(alpha) GAL4* virgin mothers. Right panel - levels of *dhd* mRNA. "*FM*" denotes the *FM7* balancer. H.) Schematic representation of proposed model of DHD-dependent redox state control at the oocyte-to-embryo transition. Dark blue color represents a highly reduced state in oocytes, where DHD levels are high. Pale blue color represents an oxidized state in embryos, where DHD levels are low. The bottom panel shows the consequences of absence of DHD.

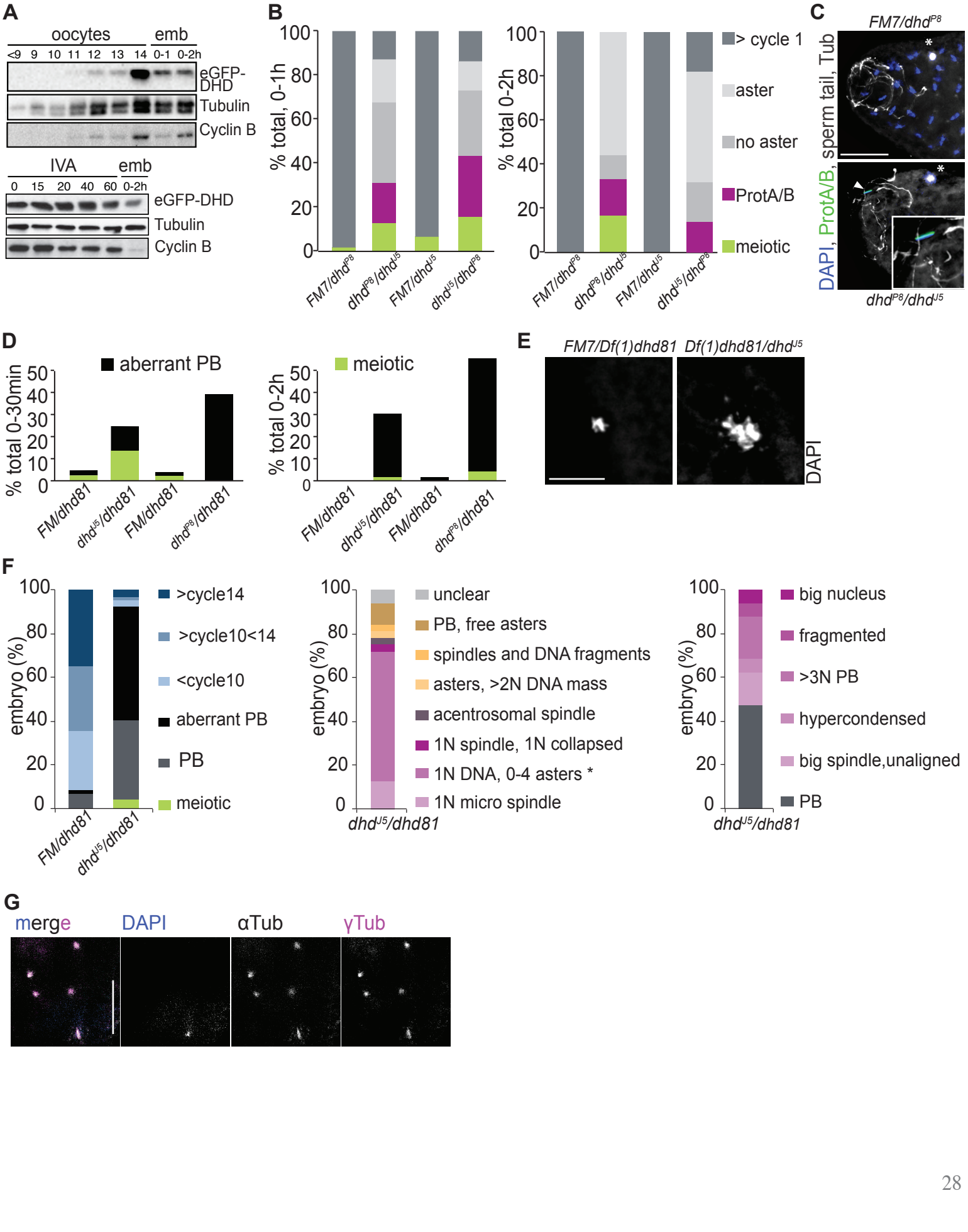
A
oocytes
emb
<9 9 10 11 12 13 14 0-1 0-2h
eGFP-DHD
Tubulin
Cyclin B
IVA
emb
0 15 20 40 60 0-2h
eGFP-DHD
Tubulin
Cyclin B
B
% total, 0-1h
% total 0-2h
> cycle 1
aster
no aster
ProtA/B
meiotic
FM7/dhdP8
dhdP8/dhdJ5
FM7/dhdJ5
dhdJ5/dhdP8
C
FM7/dhdP8
DAPI, ProtA/B, sperm tail, Tub
dhdP8/dhdJ5
D
aberrant PB
meiotic
% total 0-30min
% total 0-2h
FM/dhd81
dhdJ5/dhd81
dhdP8/dhd81
E
FM7/Df(1)dhd81
Df(1)dhd81/dhdJ5
DAPI
F
embryo (%)
>cycle14
>cycle10<14
<cycle10
aberrant PB
PB
meiotic
unclear
PB, free asters
spindles and DNA fragments
asters, >2N DNA mass
acentrosomal spindle
1N spindle, 1N collapsed
1N DNA, 0-4 asters *
1N micro spindle
big nucleus
fragmented
>3N PB
hypercondensed
big spindle,unaligned
PB
dhdJ5/dhd81
G
merge
DAPI
αTub
γTub

Fig. S6. DHD is required for faithful execution of meiosis in addition to its role in sperm decondensation. A.) Western blot analysis of extracts from various stages of oogenesis and 0-1h or 0-2h early embryos (emb) or from different time points after *in vitro* activation (IVA) of stage 14 oocytes. The oocytes and embryos were recovered from females with *eGFP-dhd* transgenes. Cyclin B levels were analyzed for comparison. α-tubulin served as a loading control. B.) Quantification of fertilization stages from 0-1h or 0-2h embryo collections from dhd^{J5}/dhd^{P8} or dhd^{P8}/dhd^{J5} mothers and corresponding sibling controls stained as in C. Only fertilized eggs were considered for analysis. "ProtA/B" – condensed sperm-head staining positive for GFP-protamine A or B. When "aster" or "no aster" were counted, decondensed DNA was associated with it. C.) 0-1h embryo collections from control $dhd^{P8}/FM7$ or sibling mutant dhd^{P8}/dhd^{J5} virgins mated to males expressing ProtA-GFP or ProtB-GFP were stained with an anti-GFP nanobody, DAPI and antibodies to visualize sperm tail and microtubules. The anterior quarter on the embryo is shown. Scale bar is 50μm. Asterisk denotes the polar body. Arrowhead indicates the condensed male sperm DNA, further enlarged in inset. D.) Quantification of polar body defects and meiosis in 0-30min or 0-2h embryo collections from *Df*(*dhd81)/dhd* ^{P8} or *Df*(*dhd81)/*dhd^{J5} mothers and corresponding sibling controls ("*dhd81*" – *Df(1)dhd81*) stained with DAPI. "*FM*" denotes the *FM7* balancer. "Meiotic" signifies the aberrant presence of meiotic stages. E.) Example of normal or aberrant polar body morphology from 0-2h embryos from *Df*(*dhd81)/+* or *Df*(*dhd81)/dhd* ^{P8} mothers, respectively. "*FM*" denotes the *FM7* balancer, "*dhd81*" – *Df(1)dhd81*. DNA is stained with DAPI. Scale bar is 20μm. F.) Quantification of defects in 0-2h embryo collections from *Df*(*dhd81)/*dhd^{J5} mothers and corresponding sibling controls ("*dhd81*" – *Df(1)dhd81*) stained with DAPI and α tubulin. Left panel - general progression through embryogenesis; middle panel – summary of non polar body defects in arrested *Df(dhd81)/*dhd^{J5} embryos according to categories (the asterisk designates phenotypes shown in panel G); right panel – breakdown of polar body defects in arrested *Df*(*dhd81)/*dhd^{J5} embryos according to categories. "PB" - presence of formed polar body. G.) dhd^{J5}/dhd ^{P8} mutant embryos were stained with DAPI and α- (αTub, grey) and γ-tubulin (γTub, magenta) antibodies. No DNA was

observed with some microtubule asters, which were often buried in the interior of the embryo. Scale bar is 20μm.

Additional supporting data excel files

Six will be submitted separately.

SUPPLEMENTARY REFERENCES

1. Kronja I, Whitfield ZJ, Yuan B, Krijgsveld J, Orr-Weaver TL (2014) Quantitative proteomic profiling of Drosophila oocyte maturation. *Proc Natl Acad Sci USA* 111:16023-16028

2. Kronja I, et al. (2014) Widespread changes in the posttranscriptional landscape at the drosophila oocyte-to-embryo transition. *Cell Rep* 7:1495–1508.

3. Tirmarche S, Kimura S, Dubruille R, Horard B, Loppin B (2016) Unlocking sperm chromatin at fertilization requires a dedicated egg thioredoxin in Drosophila. *Nat Comms* 7:13539.

4. Emelyanov AV, Fyodorov DV (2017) Thioredoxin-dependent disulfide bond reduction is required for protamine eviction from sperm chromatin. *Genes & Development* 30:2651–2656.

5. Thummel CS, Pirrotta V (1992) Technical notes: new pCasper P-element vectors. *Drosophila Information Service* 71:150.

6. Courtot C, Fankhauser C, Simanis V, Lehner CF (1992) The Drosophila *cdc25* homolog *twine* is required for meiosis. *Development* 116:405-416.

7. Schüpbach T, Wieschaus E (1989) Female Sterile Mutations on the Second Chromosom of *Drosophila melanogaster.* I. Maternal Effect Mutations. *Genetics* 121: 101–117.

8. Shamanski FL, Orr-Weaver TL (1991) The Drosophila *plutonium* and *pan gu* genes regulate entry into s phase at fertilization. *Cell* 66: 1289-1300.

9. Page AW, Orr-Weaver TL (1997) Activation of the meiotic divisions in Drosophila oocytes. *Dev Biol* 183:195–207.

10. Mahowald AP, Goralski TJ, Caulton JH (1983) *In vitro* activation of Drosophila eggs. *Dev Biol* 98:437–445.

11. Horner VL, Wolfner MF (2008) Mechanical stimulation by osmotic and hydrostatic pressure activates Drosophila oocytes *in vitro* in a calcium-dependent manner. *Dev Biol* 316:100–109.

12. Hara M, Petrova B, Orr-Weaver TL (2017) Control of PNG kinase, a key regulator of mRNA

translation, is coupled to meiosis completion at egg activation. *eLife* 6:e22219–22.

13. Hara M, et al. (2018) Identification of PNG kinase substrates uncovers interactions with the translational repressor TRAL in the oocyte-to-embryo transition. *eLife* 7:360.

14. Choi H, et al. (2011) SAINT: Probabilistic scoring of affinity purification - mass spectrometry data. *Nat Meth* 8:70–73.

15. Yang J, et al. (2015) Global, in situ, site-specific analysis of protein S-sulfenylation. *Nat Protoc* 10:1022–1037.

16. Fu L, et al. (2017) Systematic and quantitative assessment of hydrogen peroxide reactivity with cysteines across human proteomes. *Mol Cell Proteomics* 16:1815–1828.

17. Smulan LJ, et al. (2016) Cholesterol-independent SREBP-1 maturation is linked to ARF1 inactivation. *Cell Rep* 16:9–18.

18. Birsoy K, et al. (2015) An essential role of the mitochondrial electron transport chain in cell proliferation is to enable aspartate synthesis. *Cell* 162:540–551.

19. Xia J, Wishart DS (2002) Using MetaboAnalyst 3.0 for comprehensive metabolomics data analysis. *Curr Protoc Bioinformatics* 55:14.10.1–14.10.91.

20. Tran SL, Welte MA (2010) *In vivo* centrifugation of Drosophila embryos. *J Vis Exp* 40:e2005.

21. Ferree PM, Barbash DA (2009) Species-specific heterochromatin prevents mitotic chromosome segregation to cause hybrid lethality in Drosophila. *Plos Biol* 7:e1000234.

22. Kim JC, et al. (2011) Integrative analysis of gene amplification in Drosophila follicle cells: parameters of origin activation and repression. *Genes & Development* 25:1384–1398.